Environmental Science and Pollution Research
https://doi.org/10.1007/s11356-024-33359-x

RESEARCH ARTICLE

# Systematic evaluation of methods for iron-impregnation of biochar and effects on arsenic in flooded soils

**Yi Sang[1] · Behrooz Azimzadeh[2] · Jessica Olsen[1] · Jessica Rappaport[1] · Scott C. Maguffin[3] · Carmen Enid Martínez[2] · Matthew C. Reid[1]**

Received: 3 July 2023 / Accepted: 12 April 2024


## Abstract

There is a need for innovative strategies to decrease the mobility of metal(loids) including arsenic (As) and cadmium (Cd) in agricultural soils, including rice paddies, so as to minimize dietary exposure to these toxic elements. Iron (Fe)-modified biochars (FBCs) are used to immobilize As and Cd in soil-water systems, but there is a lack of clarity on optimal methods for preparing FBCs because there are only limited studies that directly compare BCs impregnated with Fe under different conditions. There is also a lack of information on the long-term performance of FBCs in flooded soil environments, where reductive dissolution of Fe (oxy)hydroxide phases loaded onto biochar surfaces may decrease the effectiveness of FBCs. This study uses material characterization methods including FTIR, SEM-EDX, BET, and adsorption isotherm experiments to investigate the effects of Fe-impregnation methods (pH, pyrolysis sequence, and sonication) on the morphology and mineralogy of Fe loaded onto the biochar surface, and to FBC adsorbent properties for arsenate (As(V)), arsenite (As(III)), and Cd. Acidic impregnation conditions favored the adsorption of As(III) onto amorphous Fe phases that were evenly distributed on the biochar surface, including within the biochar pore structure. The combination of sonication with acidic Fe-impregnation conditions led to the best adsorption capacities for As(V) and As(III) (4830 and 11,166 μg As $g^{-1}$ biochar, respectively). Alkaline Fe-impregnation conditions led to the highest Cd adsorption capacity of 3054 μg Cd $g^{-1}$ biochar, but had poor effectiveness as an As adsorbent. Amending soil with 5% (w/w) of an acid-impregnated and sonicated FBC was more effective than an alkaline-impregnated FBC or ferrihydrite in decreasing porewater As concentrations. The acid-impregnated FBC also had greater longevity, decreasing As by 54% and 56% in two flooded phases, probably due to the greater stability of Fe(III) within the biochar pore structure that may have a direct chemical bond to the biochar surface. This study demonstrates that FBCs can be designed with selectivity towards different As species or Cd and that they can maintain their effectiveness under anaerobic soil conditions. This is the first study to systematically test how impregnation conditions affect the stability of FBCs in soils under multiple drying-rewetting cycles.

**Keywords** Iron-modified biochar · Arsenic · Cadmium · Adsorption · Iron speciation · Biochar stability

## Introduction

The past decade has seen enormous growth in the use of biochar (BC) as a soil amendment to advance a wide range of agronomic and environmental goals including greater retention of water and nutrients, improvement of crop yields, mitigation of greenhouse gas emissions, and reducing the bioavailability of toxic metal(loid)s via adsorption (Lehmann & Joseph 2015). Biochar is produced by pyrolyzing organic feedstocks under oxygen-limited conditions (Cha et al. 2016, El-Naggar et al. 2019, Lehmann et al. 2011, Lyu et al. 2020), and many of its benefits for soil health are related to

Responsible Editor: Philippe Garrigues

✉ Matthew C. Reid
mcr239@cornell.edu

[1] School of Civil and Environmental Engineering, Cornell University, Ithaca, NY 14853, USA

[2] Soil and Crop Sciences, School of Integrative Plant Science, College of Agriculture and Life Sciences, Cornell University, Ithaca, NY 14853, USA

[3] Earth and Atmospheric Sciences, SUNY-Oneonta, Oneonta, NY 13820, USA

Published online: 02 May 2024

characteristic BC properties including high surface area, porous structure, and rich functional group density (Tan et al. 2015, Yu et al. 2019). In order to improve the selectivity of BC for the adsorption of metal(loid)s with a range of physical-chemical properties, a number of BC modification techniques have been implemented to "tune" BC surface properties for enhanced adsorption of specific elements (Gong et al. 2022).

There has been a particular focus on BC-modification techniques to improve the adsorption of arsenic (As). Arsenic is a non-threshold carcinogen that is widespread in terrestrial and aquatic environments (Chen et al. 2019b, Li et al. 2019), and there is particular interest in methods to decrease the bioavailability of As in rice paddy environments due to high levels of inorganic As uptake by rice plants and resulting contamination of the food chain (Zhao et al. 2010). Unmodified or pristine BC is a poor adsorbent for As, due in part to electrostatic repulsion between oxyanionic arsenate (As(V)) and the negatively charged BC surface (Zoroufchi Benis et al. 2020). Many techniques to improve BC adsorption of As have focused on impregnating BC surfaces with iron (Fe) to produce Fe-modified biochars (FBCs). Iron (oxyhydr)oxide minerals including ferrihydrite, goethite, and hematite have a high affinity and capacity for As, and the adsorption of As onto Fe (oxyhydr)oxide mineral surfaces plays a key role in controlling As mobility in natural soil-water systems (Dixit & Hering 2003, Giménez et al. 2007, He et al. 2018). Deposition of Fe (oxyhydr)oxide minerals, with typical points of zero charge (PZC) between 7.5 and 9.5 (Antelo et al. 2005, Cornell & Schwertmann 2003), on BC surfaces can also increase the surface charge which promotes adsorption of As(V) but may have less of an impact on adsorption of trivalent arsenite (As(III), pKa = 9.2) which is uncharged in most soil conditions (Dixit & Hering 2003)

A number of systematic reviews of Fe-impregnation approaches to improve BC adsorption of As have been published in recent years (Li et al. 2017b, Sun et al. 2022b, Zhang et al. 2023, Zoroufchi Benis et al. 2020). Key variables in the Fe-impregnation process that impact the physiochemical and adsorbent properties of FBCs include impregnation pH, the use of pre- or post-pyrolysis impregnation and/or the use of secondary pyrolysis, and the use of sonication (Table 1). However, a limitation of the current research is that the large majority of research typically focuses on a single type of biochar or biochar modification method per study. It is therefore difficult to determine optimal methods for Fe impregnation and make systematic comparisons. For example, it is common for studies to characterize FBCs prepared under either acidic (He et al. 2018, Hu et al. 2015, Xu et al. 2020) or alkaline (Alchouron et al. 2020, Braghiroli et al. 2020, Calugaru et al. 2019, Kim et al. 2019) conditions, but there is a lack of research that directly compares FBCs prepared under acidic or alkaline conditions, making it difficult to assess the impact of impregnation pH on FBC physiochemical properties. The lack of uniformity in BC production (e.g., feedstock, pyrolysis temperature, and other examples in Table 1) further limits the ability to compare FBC properties across multiple studies. In our research, we maintain consistency by using the same raw materials and pyrolysis procedure across all experiments. This uniformity allows us to conduct a more controlled and comparative analysis of biochar performance under various conditions. Our methodology enables a comprehensive understanding of how different treatment conditions impact biochar characteristics, setting our study apart in its ability to provide a systematic and comparative insight into biochar functionality. There has also been relatively little attention to potential tradeoffs between efforts to enhance the adsorption of As and effects on the adsorption of cationic elements like

**Table 1** Differences in Fe-modified biochar preparation methods in selected recent studies, organized by impregnation variables tested

| Variables | Treatment | Reference |
|---|---|---|
| pH | Acidic | (He et al. 2018, Hu et al. 2015, Xu et al. 2020) |
| | Alkaline | (Alchouron et al. 2020, Braghiroli et al. 2020, Calugaru et al. 2019, Kim et al. 2019) |
| | Neutral | (Huang et al. 2020, Rahman et al. 2022) |
| Pyrolysis sequence | Pre-pyrolysis treatment | (Singh et al. 2020, Zhang et al. 2019) |
| | Post-pyrolysis treatment | (Rahman et al. 2022, Zhang et al. 2019) |
| | Double pyrolysis | (Khan et al. 2020, Sun et al. 2019) |
| Iron material | $FeCl_3$ | (Calugaru et al. 2019, He et al. 2018, Singh et al. 2020) |
| | $Fe(NO_3)_3$ | (Hu et al. 2015, Khan et al. 2020, Zhu et al. 2020a) |
| | $FeSO_4{\cdot}7H_2O$ | (Rahman et al. 2020, Wu et al. 2018) |
| Pyrolysis temperature | ≤ 300 ℃ | (Lata et al. 2019, Xu et al. 2020, Zhu et al. 2020b) |
| | 300–500 ℃ | (Braghiroli et al. 2020, Guo et al. 2019) |
| | > 500 ℃ | (Khan et al. 2020, Xu et al. 2020) |
| Other | Ultrasonication | (Fan et al. 2018, Khan et al. 2020, Li et al. 2017a) |

cadmium (Cd). Cd is a common co-contaminant with As in agricultural soil and is also a major food chain contaminant (Kubier et al. 2019). Differences in the charge of As(V) and Cd lead to divergent impacts of adsorbent surface charge on adsorbent performance and can make it difficult for soil amendments to immobilize both As and Cd (Abdelrhman et al. 2022, Hartley et al. 2004, Yin et al. 2017).

The objective of this study is to determine methods for FBC preparation that optimize adsorbent performance for As, while considering potential tradeoffs with adsorption of cationic contaminants like Cd. This requires a well-controlled and systematic evaluation of Fe impregnation variables (e.g., pH, pyrolysis sequence, and use of sonication) with the same BC feedstock and pyrolysis temperature, an analysis that is currently lacking in the literature. We evaluate how different preparation methods affect the Fe phase and morphology on the BC surface and also investigate how FBC preparation methods impact the longevity of FBCs in flooded paddy soils, where the reductive dissolution of Fe (oxy)hydroxides may alter BC surface properties and decrease its long-term effectiveness in immobilizing As (Sun et al. 2022a, Yang et al. 2022). We aim to link the properties of these biochars with their performance in soil environments, particularly under the stress of multiple flooding and drying cycles. This work fills a gap in the literature on the direct comparison of FBCs prepared with a range of impregnation conditions.

## Materials and methods

### Biochar preparation

BC was prepared by pyrolyzing ash (genus *Fraxinus*) woodchips in a muffle furnace at 600 ℃. Further details on the pyrolysis conditions are in SI. After pyrolysis, most of the BC was ground into a 500–710-µm particle size, with an unground portion set aside. Table 2 summarizes eleven impregnation methods that were designed to assess the impact of various iron modification processes on the physiochemical properties of FBCs. The first set of FBCs aimed to determine the effect of Fe concentration by soaking BC in a Fe(III) solution, prepared from $Fe(NO_3)_3{\cdot}9H_2O$, at concentrations of 0.1, 0.5, 1, and 2M (resulting in FBC1-0.1, FBC1-0.5, FBC1-1, and FBC1-2, respectively) at pH ~ 0–1.

The second set of FBCs evaluated the effect of pH by comparing FBC1-1 (acidic), FBC2 (neutral), and FBC3 (alkaline). FBC2 and FBC3 were prepared with 1 M Fe at neutral (pH 7) and alkaline (pH 10) conditions (Kim et al. 2019), respectively, by adjusting pH with NaOH pellets. The impact of pH was assessed because Fe (oxyhydr) oxide mineralogy is influenced by the synthesis pH, and Fe impregnation methods have been reported in the literature at a wide range of pH (Calugaru et al. 2019, Hu et al. 2015, Huang et al. 2020).

The third set of FBCs was designed to compare the effect of pyrolysis sequence (i.e., impregnation with Fe before or after pyrolysis) on the Fe content and mineralogy of iron oxides on the biochar surface (Baig et al. 2014, Zhang et al. 2019). To control the effect of BC particle size in the FBC modification processes, both FBC4 and FBC5 used unground woodchip/biochar chips, respectively, and they were soaked in the 1 M acidic Fe impregnation solution. Then, they were subsequently ground to match the particle size of the others.

The fourth set of FBCs was prepared to explore the effects of ultrasonication and additional pyrolysis on the properties of FBCs. FBC6 was prepared using the same approach as FBC1-1, with the addition of ultrasonication during the impregnation phase to assess its effects on increasing the iron content and surface area of FBCs (Khan et al. 2020). Finally, a second pyrolysis was applied to the FBC6 to obtain FBC7, aimed at studying the effect of a second pyrolysis on iron phase transformation and impacts on As and Cd adsorption capacity (Xu et al. 2021).

**Table 2** Summary of biochar preparation methods, surface area, and Fe content of produced Fe-modified biochars. The ranges of the amorphous Fe and total Fe were indicated in brackets

| Biochar | Feedstock | Fe solution concentration | Impregnation sequence | pH | Other treatment | Surface area ($m^2$/g) | Total Fe content (mg/g) | Amorphous Fe content (mg/g) |
|---|---|---|---|---|---|---|---|---|
| FBC1-0.1 | Ground biochar | 0.1 M | Post-pyrolysis | 1.34 | | 13.48 | 4.63 (4.31–4.96) | 2.67 (2.51–2.83) |
| FBC1-0.5 | Ground biochar | 0.5 M | Post-pyrolysis | 0.62 | | 3.40 | 21.88 (20.99–22.77) | 17.75 (17.49–18.02) |
| FBC1-1 | Ground biochar | 1 M | Post-pyrolysis | ~ 0 | | 4.32 | 28.20 (28.08–28.31) | 23.65 (23.37–23.93) |
| FBC1-2 | Ground biochar | 2 M | Post-pyrolysis | ~0 | | 3.73 | 51.82 (51.07–52.58) | 51.22 (50.99–51.45) |
| FBC2 | Ground biochar | 1 M | Post-pyrolysis | 7 | | 137.81 | 9.78 (9.48–10.09) | 9.48 (9.22–9.74) |
| FBC3 | Ground biochar | 1 M | Post-pyrolysis | 10 | | 75.60 | 30 (29.76–30.24) | 18.75 (18.57–18.92) |
| FBC4 | Unground woodchip | 1 M | Pre-pyrolysis | ~ 0 | | 256.82 | 5.17 (4.89–5.46) | 5.05 (5.00–5.09) |
| FBC5 | Unground biochar | 1 M | Post-pyrolysis | ~ 0 | | 5.22 | 24.97 (24.40–25.65) | 26.66 (25.59–27.74) |
| FBC6 | Ground biochar | 1 M | Post-pyrolysis | ~ 0 | Sonication | 11.22 | 95.62 (89.42–101.82) | 70.32 (68.71–71.93) |
| FBC7 | Ground biochar | 1M | Double pyrolysis | ~ 0 | Sonication | 369.77 | 98.39 (98.34–98.44) | 25.55 (25.06–26.03) |
| Pristine biochar | Unground woodchip | N/A | N/A | N/A | | 507.56 | 0.05 (0.01–0.08) | 0.02 (0.01–0.02) |

## Biochar characterization

The concentration of amorphous and total iron concentrations of FBCs were determined using acid ammonium oxalate extraction (Seyfferth et al. 2014) and extraction with 6M HCl and 6M $HNO_3$ in duplicate, respectively. The crystalline Fe content was calculated as the difference between total and amorphous Fe. The specific surface area was measured using BET analysis (Quantachrome Autosorb iQ Analyzer, Boynton Beach, FL), and the Fe mineral phases were identified using XRD (Bruker D8 Advance ECO powder diffractometer). The surface bonding environment was characterized by collecting Fourier-transform infrared (FTIR) spectra with a Bruker Vertex 70 spectrometer equipped with a Pike GladiATR accessory (Bruker Optics Inc., Billerica, MA, USA; Pike Technologies, Madison, WI, USA). FTIR spectra were collected before and after a pH adjustment to pH 7, focusing on the range of 1800–200 $cm^{-1}$ due to its relevance for biochar and Fe (oxy)hydroxides. The morphology and elemental distribution of FBCs were analyzed by scanning electron microscopy (SEM, Zeiss Gemini 500 Scanning Electron Microscope) and energy dispersive spectroscopy (EDS).

## Adsorption isotherms

Duplicate adsorption isotherm experiments were conducted in 15-mL centrifuge tubes at room temperature (22 °C). As(V) and As (III) solutions were prepared with initial As concentrations of 750, 3000, 9000, 12,000, 24,000, 48,000, 75,000, and 112,500 µg As $L^{-1}$ in a matrix consisting of 5 mM $KNO_3$ and 10 mM $NaHCO_3$. For Cd adsorption experiments, solutions were prepared in a matrix of 5 mM $KNO_3$ and 5 mM MOPS (to avoid $CdCO_3$ precipitation) with initial cadmium concentrations of 100, 1000, 4500, 9000, 13,500, 18,000, 25,000, and 35,000 µg Cd $L^{-1}$. The pH was adjusted to 7.0 ± 0.1 for all experiments. To conduct the adsorption experiments, 20 mg of BC was added to 10 mL solution of As(V), As(III), or Cd(II), and mixing on a rotary shaker for 48 h. The solution was then filtered through 0.22-µm PES filters and analyzed using ICP-MS. As(III) adsorption experiments were performed in an anaerobic chamber (Coy Laboratories, 96% $N_2$/4% $H_2$, < 10 ppm $O_2$).

In order to study the maximum adsorption capacity and adsorption affinity, adsorption isotherm results were fit with both Langmuir (Eq. 1) and Freundlich (Eq. 2) models (Sparks 2003) using the following equations:

$$q_e = \frac{Q_{max} K_{ads} C_e}{1 + K_{ads} C_e} \quad (1)$$

$$q_e = K_F \{C_e\}^N \quad (2)$$

where $q_e$ and $C_e$ represent the adsorbed concentration (µg adsorbate $g^{-1}$ adsorbent) and adsorbate concentration at equilibrium (µg adsorbate $L^{-1}$), respectively. The Langmuir isotherm is controlled by two constants. $K_{ads}$ (L $g^{-1}$) is the affinity of the adsorbent for adsorbate $Q_{max}$ (µg $g^{-1}$) is the maximum adsorption capacity. The Freundlich model is defined by $K_F$ (µg $g^{-1}$) (L $\mu g^{-1})^N$, an indicator of the adsorbent affinity for sorbates, and $N$, a unitless parameter describing how the binding strength changes with the change of adsorption density.

## Soil microcosm experiments

Two types of soils were used in microcosm experiments to test the effectiveness of FBCs as soil adsorbents over multiple drying-rewetting cycles. A rice paddy soil (hereafter, paddy soil) from the mid-South U.S. rice production region was collected in Stuttgart, Arkansas (Maguffin et al. 2020, Zhang & Reid 2022). A sewage sludge-contaminated soil (hereafter, orchard soil) was collected from the Cornell Apple Orchards in Ithaca, NY (Richards et al. 1998, Udovic & McBride 2012). Both soils were air-dried and sieved through a 2-mm sieves. A total elemental analysis of the soils was performed using a modified version of EPA method 3051-6010. The organic matter content of both soil samples was measured via loss on ignition (LOI) (Heiri et al. 2001).

The soil microcosm experiments were conducted by adding 200 g soil and 2g air-dried and coarsely ground leaves as an organic matter source, with 10 different treatments conducted in triplicate. FBC3 and FBC6 were chosen to be applied in soil experiments due to their high Cd and As adsorption capacity, respectively, as well as their differing Fe mineralogy. The 10 treatments were as follows: (1) unamended orchard soil, (2) orchard soil with 1% (w/w) FBC3, (3) orchard soil with 5% (w/w) FBC3, (4) orchard soil with 1% (w/w) FBC6, (5) orchard soil with 5% (w/w) FBC6, (6) orchard soil with synthetic ferrihydrite, (7) unamended paddy soil, (8) paddy soil with 1% (w/w) FBC6, (9) paddy soil with 5% (w/w) FBC6, and (10) paddy soil with synthetic ferrihydrite. The ferrihydrite experiments were intended to compare the effectiveness and longevity of FBC to an amorphous Fe (oxy)hydroxide mineral. Ferrihydrite was synthesized following the procedure described in Smith et al. (2012) and the mineralogy was confirmed by XRD (Figure S1). Then, 0.95g ferrihydrite was applied to the soils to have an equivalent Fe concentration as the 5% (w/w) FBC6. Microcosms were staged in an environmental chamber at 26 ℃ with 60% humidity and were flooded with a media containing 0.5 mM NaCl and 1 mM $NaHCO_3$, adjusted to pH 7. A constant water level of 2–3 cm above the soil surface was maintained. Microcosms were maintained under flooded conditions for 5 weeks before being dried for

2 weeks via evaporation. A second 6-week flood period was then conducted to examine how the FBC performed over 2 consecutive flood periods. Porewater samples were collected weekly using a Rhizon porewater sampler. Additional FBC3 or FBC6 were placed in mesh bags and buried in the orchard soil and were then retrieved at three different time points to characterize the effects of the soil aging process on FBC surface properties.

Elemental concentrations (As, Cd, Fe, and Mn) of porewater were measured via ICP-MS (Agilent 7800). Major cation and anion concentrations were measured using ion chromatography (Dionex ICS-2100). Soil pH was measured by inserting the pH probe (Orion 9107WMMD) into the surficial soil. DOC and DIC were measured at the beginning and the end of the flooded period with a TOC-L Total Organic Carbon Analyzer (Shimadzu). S(-II) concentration was measured using the Cline method (Cline 1969).

## Results and discussion

### Effect of impregnation media pH on Fe-loading and morphology

FBC1-1, FBC2, and FBC3 were produced to provide a comparison of the effect of impregnation under acidic, neutral, and alkaline conditions on FBC physiochemical properties. The total surface area, along with the total and amorphous Fe content of these FBCs, is summarized in Table 2. FBC1-1, synthesized under acidic conditions, had the smallest surface area of 4.32 $m^2g^{-1}$, while FBC2, prepared under the neutral condition, had the largest surface area of 137.81 $m^2g^{-1}$, and the FBC3 had a surface area of 75.6 $m^2g^{-1}$. FBC3 had a slightly higher total Fe content of 30 mg $g^{-1}$ than FBC1-1, which had a total Fe content of 28.2 mg $g^{-1}$. However, FBC1-1 had more amorphous Fe (23.65 mg $g^{-1}$) compared to FBC3 (18.75 mg $g^{-1}$). FBC2 had the lowest total Fe content of 9.78 mg $g^{-1}$ and amorphous iron content of 9.48 mg $g^{-1}$. XRD data (Figure S1) indicate that the Fe phases in FBC1-1 and FBC3 were primarily ferrihydrite and goethite, respectively. The XRD pattern for FBC2 did not show any clear iron oxide peak, consistent with the high amorphous iron fraction of the low overall iron content. ATR-FTIR spectra (Fig. 1) indicates that characteristic ferrihydrite peaks at ~ 1338 and ~ 705 $cm^{-1}$ were found in FBC1-1, and characteristic goethite peaks at 894/792 and 635/388/259 $cm^{-1}$ were found in both FBC1-1 and FBC3 (Blanch et al. 2008, Cornell & Schwertmann 2003). Weak Ferrihydrite peaks were also found in FBC2.

SEM-EDS imaging showed that impregnation pH had a major impact on the morphology of Fe on the BC surface and the distribution of Fe within the BC pore structure. FBC3, which was prepared at pH 10, was characterized by large Fe aggregates on the BC surface (Fig. 2B). Nucleation and precipitation of iron oxides occur faster in neutral and alkaline conditions compared to acidic conditions, likely decreasing the diffusion of Fe into the BC pore structure, and contributing to the higher surface area in FBC3. Another factor that could have contributed to the higher surface area, distinct from pH effects on Fe solubility, is the effect of alkaline treatment on removing impurities from and/or opening nanopore structures (Ji et al. 2010, Jin et al. 2014, Regmi et al. 2012). Under pH 10, $Fe(OH)_4^-$ was the dominant Fe(III) species in the solution, and its solubility is higher than $Fe(OH)_3$ but lower than $Fe^{3+}$ (Furcas et al. 2022, Jolivet et al. 2004). As a result, FBC3 had uneven Fe distribution on its surface due to the low solubility of $Fe(OH)_4^-$ at pH 10 and only limited diffusion into the pore structure. In contrast, the acidic impregnation conditions of FBC1-1 led to greater Fe solubility and a more even distribution of Fe on the BC surface as well as the pore structure.

The adsorption performance of FBC1-1, FBC2, and FBC3 for As(V) and As(III) is shown in Fig. 3, and model parameters for both Langmuir and Freundlich isotherm models are summarized in Table S2. Adsorption capacity ($q_{max}$) for both As(V) and As(III) decreased in the order FBC1-1 (acidic impregnation) > FBC3 (alkaline impregnation) > FBC2 (neutral impregnation). FBC2 had particularly poor adsorbent properties, with a $q_{max}$ for As(V) less than 500 µg As $g^{-1}$ BC. As(III) sorption isotherm experiments were not conducted for FBC2 due to its low As(V) adsorption capacity. This rank order of $q_{max}$ across the FBCs prepared at different pH was more closely related to the amorphous Fe content than total Fe content and was not related to the surface area. FBC3 prepared under alkaline conditions had the highest Cd adsorption capacity, with a $q_{max}$ for Cd(II) at 3053 µg $g^{-1}$. Fan et al. (2018) indicated that the amorphous Fe on biochar was associated with substantial amount of As through sequential extraction experiments. Acidic impregnation conditions were shown to produce a greater total Fe content and a greater amorphous fraction compared to neutral and alkaline conditions (Fig. S2), consistent with FTIR analysis showing that highly amorphous ferrihydrite was the dominant Fe phase in FBC1-1. This comparison of impregnation pH indicates that acidic impregnation conditions produce FBC with better adsorbent properties compared to neutral or alkaline conditions due to pH effects on Fe loading to the BC surface and the amorphous fraction of the Fe.

While there has been extensive previous research on FBCs, as summarized in Table 1 (Alchouron et al. 2020, He et al. 2018, Hu et al. 2015, Huang et al. 2020, Kim et al. 2019), there is limited information on how different impregnation pH with the same feedstock impacts adsorbent properties. Calugaru et al. (2019) prepared FBCs at pH 8.5 and 12 and determined that the FBC prepared at pH

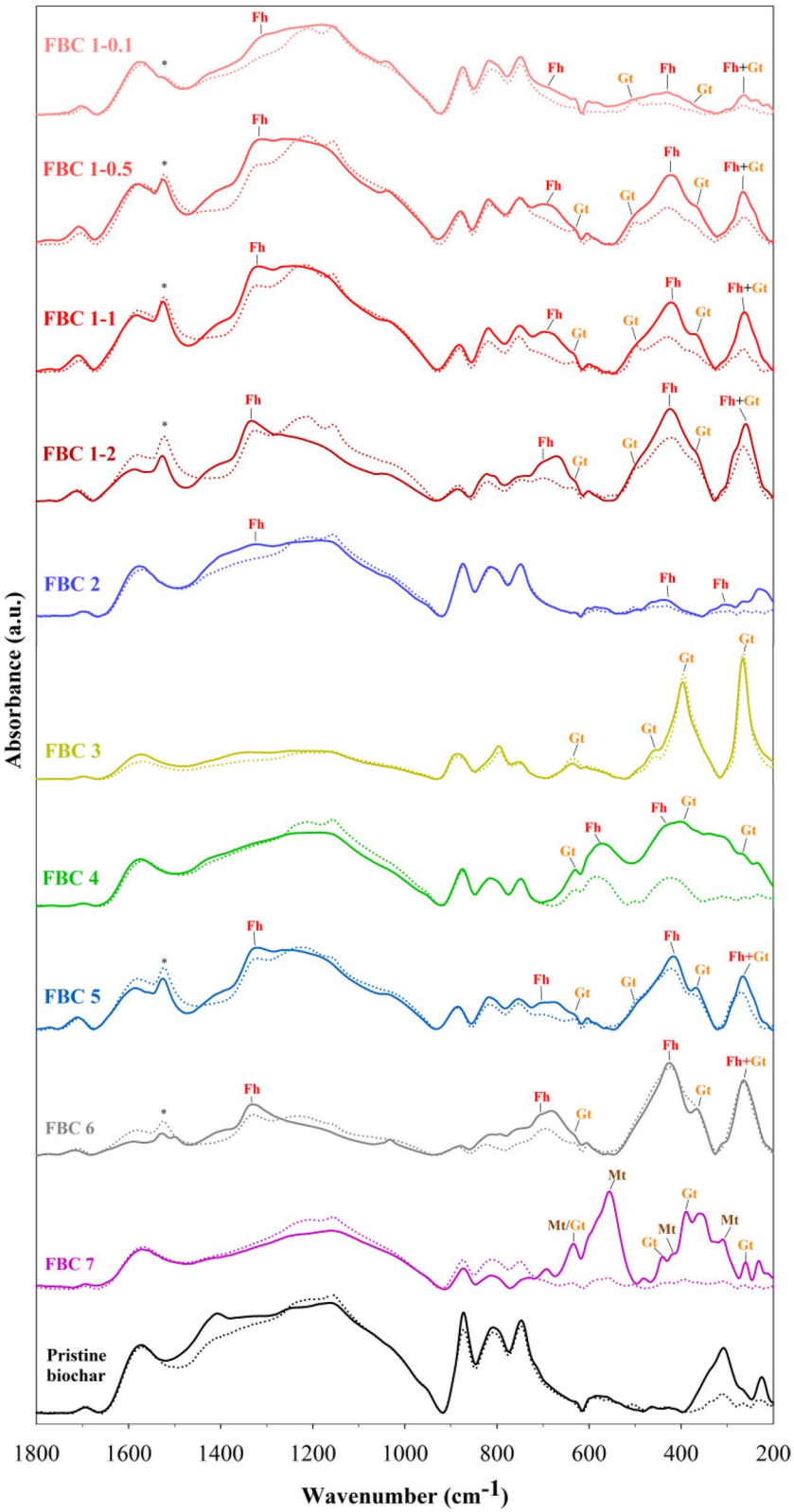


**Fig. 1** FTIR spectra of pristine biochar and FBCs. Solid lines show spectra of FBCs used in experiments, while dotted lines show spectra of FBCs after adjustment to pH 7. The peak positions of precipitated Fe (oxy)hydroxides (Gt, goethite; Fh, ferrihydrite; and Mt, magnetite) are denoted on FBC spectra based on pure laboratory-synthesized minerals (reference FTIR spectra shown in Figure S5). The peak indicated by asterisks is unidentified while closely associated with the post-pyrolysis acidic iron impregnation biochar

12 performed better in As(V) adsorption due to the different PZC. However, they did not compare FBCs prepared under acidic conditions. Here, we show BC impregnation under acidic conditions led to better arsenic adsorption. The formation of amorphous Fe and crystalline Fe can be controlled by various factors (e.g., pH, reaction time, and

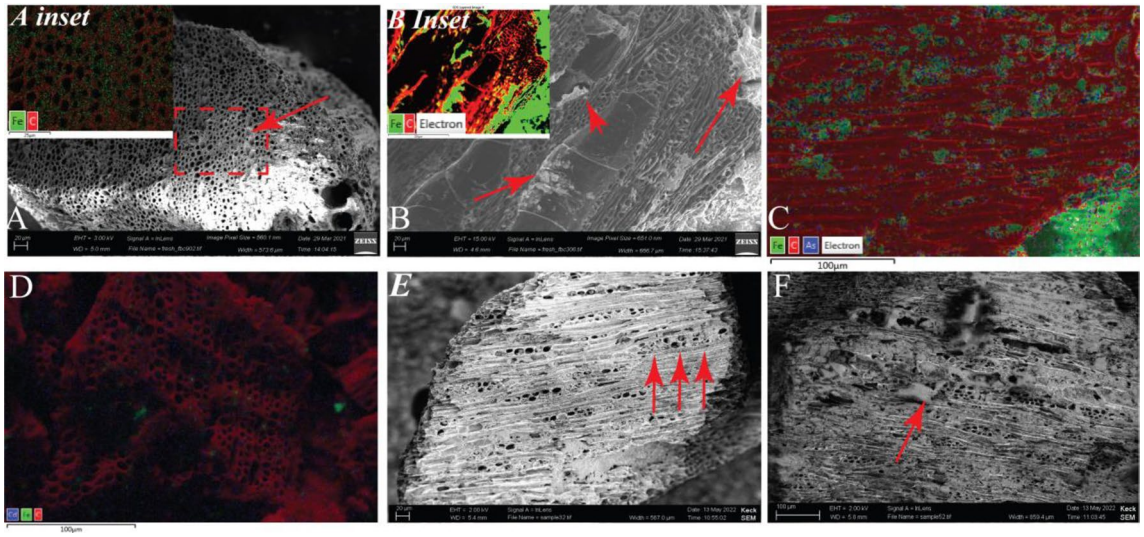


**Fig. 2** SEM-EDS imaging of select FBCs. **A** SEM image of FBC6, showing uptake of Fe into the BC pore structure. The inset shows EDS mapping of the FBC surface and shows the uniform distribution of Fe on the BC surface. **B** The SEM image of FBC3. Arrows indicate large mineral aggregates on the BC surface, which were not identified on the surface of FBC6. The inset shows EDS mapping of FBC3 and shows large Fe aggregates which were not identified on FBC6. **C** SEM-EDS image of As adsorption on FBC1-1 retrieved from sorption isotherm experiment, showing the co-location of As with Fe. **D** SEM-EDS image of Cd adsorption on FBC1-1. **E** SEM image of FBC6 at the end of the second flood phase in the soil microcosm experiments. Arrows show similar morphology of Fe taken up in the pore structure. **F** The SEM image of FBC3 at the end of the first flood phase, showing persistence of Fe aggregates on the BC surface under anaerobic incubation conditions

temperature). Generally, amorphous Fe oxides are more likely to form under acidic to neutral pH with a rapid hydrolysis (Cornell & Schwertmann 2003). Baltpurvins et al. (1996) indicated that at higher pH, the transformation from freshly precipitated iron(III) oxides sludges to more crystalline Fe species (e.g., goethite) will be faster.

## Effects of impregnation media Fe concentration and sonication on Fe loading and morphology

A range of Fe concentrations in the acidic impregnation solution were tested to evaluate the impact on surface Fe loading. An increase in the Fe(III) concentration from 0.1 to 0.5 M, 1 M, and 2 M (FBC1-0.1, FBC1-0.5, FBC1-1, and FBC 1-2) led to an increase in total iron content from 4.63 to 51.82 mg $g^{-1}$. The amorphous Fe content increased from ~ 60% in the FBC1-0.1 sample to nearly 100% in the FBC1-2 sample. The increase in both total and amorphous Fe correspondingly led to an enhanced adsorption of As(V) (Fig. S3). The surface area decreased as Fe loading increased, which is consistent with SEM imaging showing that Fe impregnation under acidic conditions led to the uptake of Fe into the pore structure and blocking of pore throats (Fig. 2).

Sonication during the Fe impregnation was effective at creating a large increase in the total iron content, amorphous iron content, and surface area. This is shown by a comparison of FBC6 and FBC1-1, where FBC6 was prepared in the same way as FBC1-1 with the addition of sonication during the impregnation process. These changes could be due to the enhanced uptake of Fe into the pore structure during sonication, or the removal of impurities produced during the pyrolysis process and trapped in nanopore structures (Luo et al. 2019, Sajjadi et al. 2019). The adsorption capacity of FBC6 for As(V) and As(III) showed a significant increase compared with FBC1-1, with a roughly 2.5-fold increase to 4830 µg $g^{-1}$ for As(V) and a 3-fold rise to 11,166 µg $g^{-1}$ for As(III). Additionally, FBC6 demonstrated an adsorption capacity of 2564 µg $g^{-1}$ for Cd(II). In comparison, Hu et al. (2015) reported an As(V) maximum adsorption capacity of 2.16 mg/g using hickory chips-based FBC, pyrolyzed with $Fe(NO_3)_3{\cdot}9H_2O$ at 600 °C for 2 h. Furthermore, Kim et al. (2019) reported a maximum As(III) capacity of 13.5 mg/g using a giant Miscanthus-based FBC. Chen et al. (2019a) investigated the Cd adsorption capacities of various biochars, finding that woodchip biochar had a maximum capacity of 3.08 mg/g and iron-loaded woodchip biochar 22.6 mg/g.

## Effects of Fe impregnation-pyrolysis sequence on Fe loading and morphology

Prior studies of FBC preparation have involved Fe-impregnation of the biomass feedstock prior to

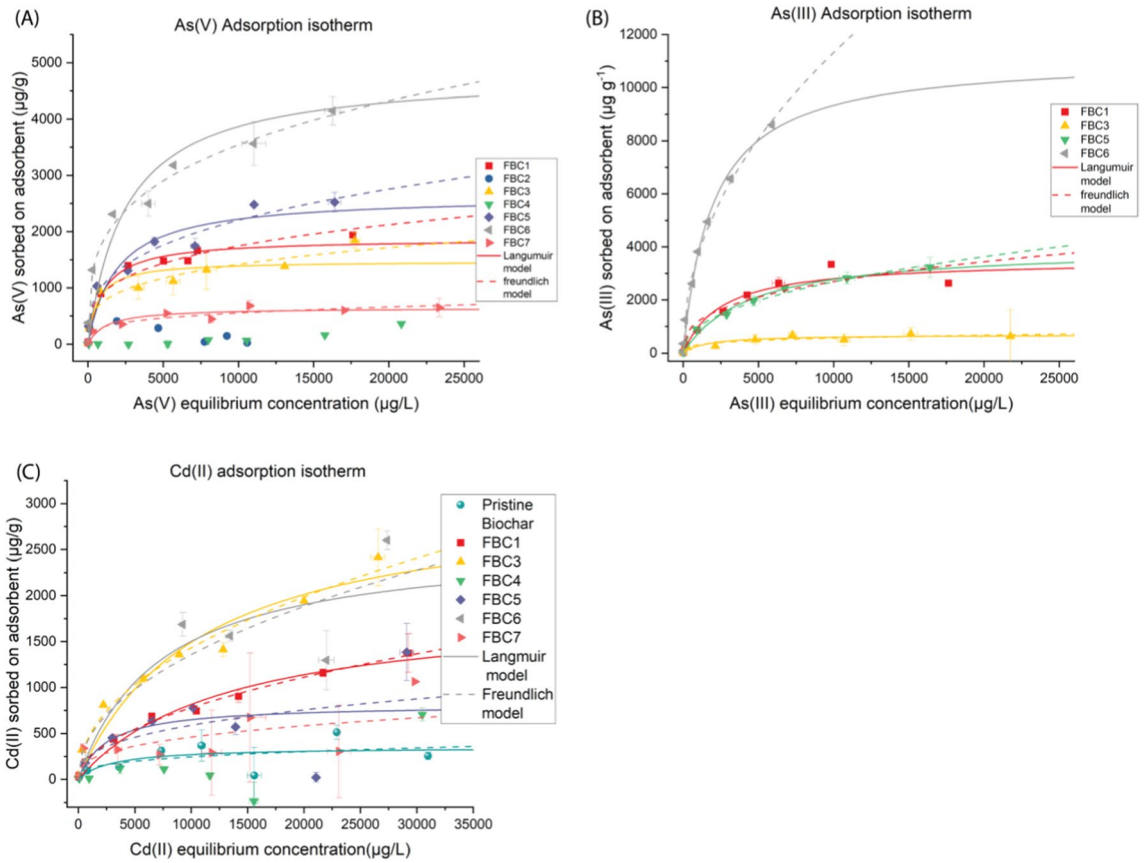


**Fig. 3** **A** As(V) adsorption isotherms and model fits with Langmuir and Freundlich models. For clarity, model fits are not shown for BCs with low As(V) adsorption capacity (< 500 μg As/g biochar). **B** As(III) adsorption isotherms and model fits with Langmuir and Freundlich models. **C** Cd adsorption isotherms and model fits with Langmuir and Freundlich models. Model parameters are summarized in Table S2. Symbols show mean of n = 2 samples and error bars show the range

pyrolysis as well as Fe-impregnation of already-pyrolyzed biomass (Table 1), and there is a lack of clarity on the effects of pyrolysis sequence on FBC properties (Khan et al. 2020, Rahman et al. 2022, Singh et al. 2020, Sun et al. 2019, Zhang et al. 2019). Here, we tested the effects of both pre- (FBC4) and post-pyrolysis (FBC5) impregnation. While the surface area of FBC4 (256.82 $m^2g^{-1}$) was much larger than the surface area of FBC5 (5.22 $m^2g^{-1}$), other properties of FBC5 made it a more favorable adsorbent. FBC5 had a greater total and amorphous Fe content of 24.97 mg $g^{-1}$ (24.40–25.65 mg $g^{-1}$) and 26.66 mg $g^{-1}$ (25.59–27.74 mg $g^{-1}$), respectively. The larger mean value of amorphous iron content than total iron content was considered as measurement error. FBC4 had much lower total and amorphous iron content of 5.17 mg $g^{-1}$ and 5.05 mg $g^{-1}$, respectively. XRD (Figure S1) and FTIR (Fig. 1) showed the presence of both ferrihydrite and goethite Fe phases on the surfaces of both FBC4 and FBC5. FBC5 had a $Q_{max}$ of 2634, 3985, and 1987 μg $g^{-1}$ for As(V), As(III), and Cd, respectively. FBC4 had poor adsorption capacities for As(V) and Cd(II), which were both lower than 500 μg $g^{-1}$. An As(III) adsorption isotherm was not conducted for FBC4 due to the poor performance with As(V) adsorption. The comparison between FBC4 and FBC5 indicates that the post-pyrolysis impregnation led to a better adsorbent for arsenic adsorption, which is differed from some prior studies. For example, Zhang et al. (2019) employed rice straw as feedstock and explored the effect of both pre- and post-pyrolysis impregnations. They found that impregnation of unpyrolyzed biomass (pre-pyrolysis impregnation) resulted in higher iron loading in FBCs and enhanced As adsorption. These different findings may be attributable to the use of different feedstocks.

A second pyrolysis step was applied to FBC6 to create FBC7 and assess the effect of a pyrolysis-impregnation-pyrolysis sequence. This led to a greater surface area and similar total Fe content, but a large decrease in the amorphous Fe content. FTIR indicated that the second pyrolysis step led to a transformation of the Fe phase from ferrihydrite to magnetite and goethite. The $Q_{max}$ for both As(V) and Cd(II) decreased sharply as a result of a

second pyrolysis to 644 μg $g^{-1}$ and 520 μg $g^{-1}$, respectively. The adsorption of As(III) was not conducted for FBC7 due to its poor As(V) adsorption performance. Previous studies have shown that a second pyrolysis step leads to the transformation of amorphous to crystalline Fe, and at a temperature of 800 ℃ can produce zero-valent iron (ZVI) (Xu et al. 2021). Here, our second pyrolysis step of 600 ℃ transformed about half of amorphous iron to crystalline iron as goethite and magnetite, without the observation of ZVI. As a result, the As and Cd adsorption capacity of FBC7 decreased with decreasing amorphous iron content. This further indicates that amorphous Fe is a more important factor than crystalline iron or total iron in controlling As and Cd adsorption.

In our study, we explain the greater uptake of Fe in the post-pyrolysis impregnation method with the greater surface area and greater amorphous iron content of the pyrolyzed BC compared to the pristine woodchip (Carrott et al. 2008, Tan et al. 2021), allowing for more retention of Fe and greater Fe surface loading.

## Effects of iron morphology on adsorbent properties

The effects of total and amorphous Fe loading, as well as surface area, on adsorption capacities for As(V), As(III), and Cd are summarized in Fig. 4. The amorphous iron content is a better predictor of $Q_{max}$ for As(V), As(III), and Cd than total Fe. The total surface area of the FBCs was not related to $Q_{max}$ for any of the analytes. It is well-established that amorphous Fe oxides have greater sorption capacities than crystalline phases due to greater Fe oxide surface areas and binding site densities (Kumar et al. 2008, Schwertmann & Murad 1983).

When comparing As(V) and As(III), it was found that acidic impregnation conditions led to greater $Q_{max}$ for As(III) than As(V), which is the same as the results indicated by Samsuri et al. (2013). Their study reported higher As(III) adsorption capacity than As(V) using the Fe-loaded fruit bunch biochar and rice husk biochar impregnated under pH 6. The biochar surface consists of a mixture of negatively charged functionalities associated with pyrolyzed biomass and Fe-O binding sites that, for ferrihydrite and goethite, are positively charged at pH 7. At pH 7, $H_3AsO_3$ is the dominant As(III) species while $H_2AsO_4^-$ and $HAsO_4^{2-}$ are both predominant As(V) species. Electrostatic repulsion between As(V) and negatively charged biomass-associated functionalities may decrease the adsorption of As(V) compared to uncharged As(III). FBC3 was characterized by discrete Fe precipitates on the biochar surface rather than a more uniform distribution of Fe on the biochar surface, including within pores, as seen for FBC6 in Fig. 2. The surface complexation reactions between As(V) and these discrete, larger Fe aggregates on the FBC3 surface may have been less influenced by the charge of organic biochar functionalities, compared to surface complexation reactions with the more uniformly distributed Fe on FBC6 and other acid-prepared biochars.

A correlation matrix of FBC physical-chemical variables shows a strong positive correlation between the amorphous Fe content and both As(V) and As(III) adsorption capacities ($r$ = 0.92 and 0.99, respectively) (Figure S4). In conclusion, amorphous Fe is a critical predictor for both As(V) and As(III) adsorption, and there is no clear tradeoff between As and Cd adsorption.

## Mechanisms controlling Fe morphology and speciation

The ATR-FTIR spectra provided evidence for the initial surface complexation of Fe(III) with O-containing functionalities on the BC surface, followed by nucleation and clustering at higher Fe loadings and at higher pH. As Fe loadings increased in the FBC1 series, the C=O peak shifted to higher wavenumbers between 1700 and 1710 $cm^{-1}$. This could be a result of an interaction between the Fe center and carbonyl in quinone/ketone moieties on the BC surface (Kassaee et al. 2011). In addition, the peak centered at 1565 $cm^{-1}$ (1665–1550 $cm^{-1}$) on the pristine BC, tentatively assigned to an overlap between the stretching vibration of aromatic C=C groups with the carbonyl stretching vibration of carboxylic acid and amide groups (Calderón et al. 2006, Cantrell et al. 2012), shifted to 1587 $cm^{-1}$ for acid-impregnated BCs. This suggests that under acidic conditions Fe atoms may form a complex through carboxyl groups at the BC surface (Bhattacharyya et al. 2019). The goethite (Gt) peak located at 388 $cm^{-1}$ shifted to a lower wavenumber as Fe loading increased in the FBC1 series (~ 364 $cm^{-1}$), indicating initial chemical bonding of Fe to the BC surface at low Fe concentration, followed by precipitation of a Gt and ferrihydrite (Fh) mixture at higher Fe loadings. Such direct bonding between poorly crystalline Fe and BC surfaces has been reported recently in Xu et al. (2022). It is therefore likely that for acid impregnation conditions the formation of Fh and Gt on the BC started as a heterogeneous nucleation process, where Fe complexation with O-containing BC functional groups was the first step followed by continuous hydrolysis and nucleation of Fe. This C-O-Fe signal will be damped as the signal from Fh/Gt becomes more prominent (Bazilevskaya et al. 2018).

In contrast to the acid-impregnated FBCs, the Gt-associated bands in alkaline-impregnated FBC3 occur at the same location and shape as the reference Gt mineral (Fig. 1; Figure S5), indicating the absence of direct chemical bonding between Fe and functional groups on the BC surface. Therefore, it is likely that FBC3 is composed of Fe (oxy)hydroxide surface precipitates with higher crystalline order or grain size, consistent with the lower amorphous

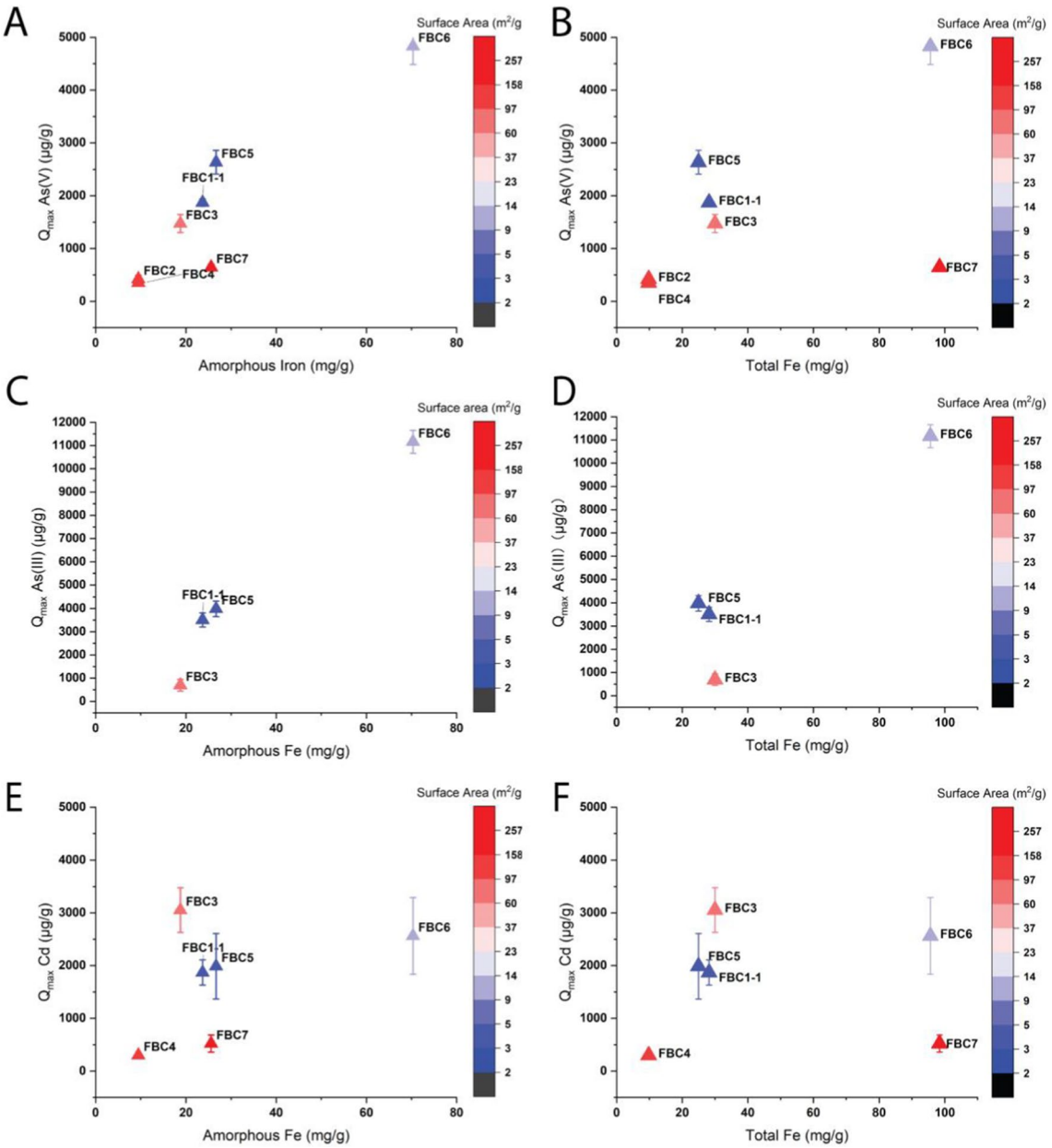


**Fig. 4** **A** $Q_{max}$ for As(V) as a function of the amorphous iron content and total surface area. **B** $Q_{max}$ for As(V) as a function of the total iron content and total surface area. **C** $Q_{max}$ of As(III) as a function of the amorphous iron content and total surface area. **D** The $Q_{max}$ of As(III) as a function of the total iron content and total surface area. **E** $Q_{max}$ of Cd as a function of the amorphous iron content and total surface area. **F** $Q_{max}$ of Cd as a function of the total iron content and total surface area. Symbols represent best-fit $Q_{max}$ values determined using non-linear regression, and error bars show the standard deviation of the model estimate

Fe fractions of these BCs (Figure S2). SEM imaging also revealed a larger grain size for FBC3 compared to FBC1 (Fig. 2). Overall, the predominant Fe mineralogy of FBC3 was Gt, while the acid-Fe soaked biochars contained mixed Fe (oxy)hydroxides (e.g., Gt and Fh) that are more effectively taken up into the pore structure and may bind to the BC surface through O-containing functional groups, especially at low Fe/BC ratios. Additional discussion of the ATR-FTIR spectra is in SI.

## Effects of FBCs on As and Cd mobilization in flooded soil microcosms

FBC3 and FBC6 were selected for soil microcosm experiments due to their differences in Fe mineralogy, amorphous Fe content, and performance as adsorbents for As vs. Cd. Synthetic ferrihydrite (Fh) was also tested as an amendment to compare the effect of FBC to a Fe (oxy)hydroxide mineral phase. Soil elemental compositions are summarized in

Table S1. Fe concentrations in the paddy and orchard soils were similar, while As and Cd were higher in the orchard soil. Only FBC6 was used in the paddy soil since paddy soil Cd concentrations were very low (0.2 mg/kg), and therefore, the Cd adsorbent properties of FBC3 were not as important.

The pH in unamended (control) paddy and orchard soils increased under flooded conditions, likely due to the reduction of Fe and Mn oxides (Figure S6). pH was between 6.5 and 7.5 in both soils after day 7. Amendment with FBC6 led to lower pH in both soils while FBC3 increased pH, most probably due to acidic vs. alkaline impregnation conditions. As and Fe concentrations in porewater increased between Days 1 and 14, and for the most part were stable between days 14 and 35 (Fig. 5). In the second flood phase, As concentrations were relatively low in the paddy soil due to lower organic carbon concentrations (Figure S7A; Table S1). The combination of greater total soil As and greater organic carbon led the orchard soil porewater to have As concentrations that were almost an order of magnitude greater than the paddy soil.

The 5% FBC and Fh amendment substantially decreased porewater As relative to the unamended control in both soils, while the 1% FBC amendments had either a small or no effect. The Fh amendment increased Fe concentrations in the orchard soil pore water relative to the control, while in the paddy soil, Fe concentrations were similar in the Fh-amended and unamended control microcosms. Notably, in the orchard soil, the 5% FBC6 and 5% FBC3 had lower Fe porewater concentrations than the unamended control, which may be due to the (re-)adsorption of Fe(II) onto the BC surface (Jeong et al. 2007). Based on our results, it is not possible to determine whether FBC-associated Fe(III) phases experienced less reductive dissolution compared to Fh, or if a similar amount of Fe(III) experienced reductive dissolution before sorbing onto BC surfaces. This distinction is important for understanding the stability of Fe(III) adsorption sites under reducing conditions. The FBCs did not inhibit sulfate reduction (Figure S8A), so impacts on Fe solubility do not appear to be related to effects on redox potential. While FBC amendment and Fh appeared to have some effect on porewater Cd concentrations in the orchard soil, these effects were small compared to the rapid decrease of Cd in all conditions upon the onset of flooded conditions (Fig. 5B), as is commonly observed in reducing soils

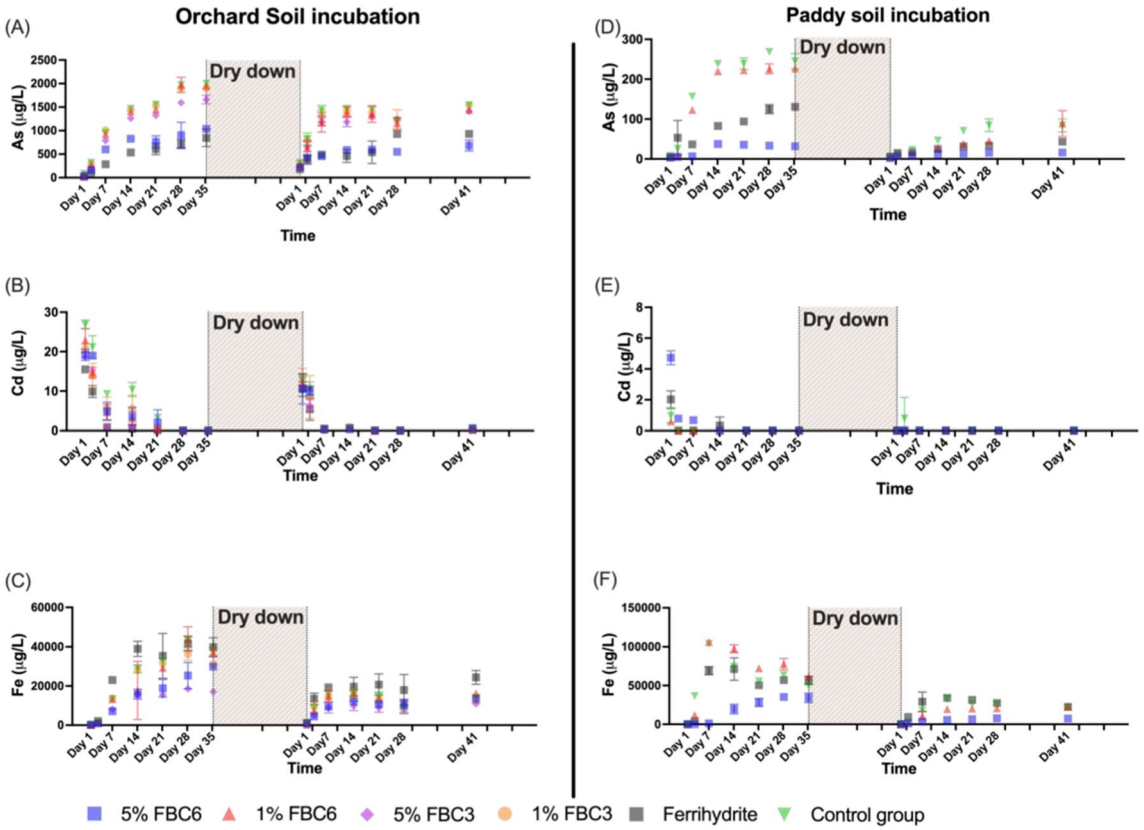


**Fig. 5** Dissolved **A** As, **B** Cd, and **C** Fe concentrations in the orchard soil pore water and dissolved **D** As, **E** Cd, and **F** Fe concentrations in the paddy soil pore water in the first and second flooded phases of soil microcosm experiments. The shaded areas represent the dry-down period between two flooding phases. Symbols show the mean of $n = 3$ replicate microcosms, and error bars show the standard deviation

(Fulda et al. 2013). Additional aspects of the Cd dynamics are described in SI.

Due to the low porewater Cd concentrations under anaerobic conditions, our analysis focuses on the effects and longevity of FBC amendment on As mobility. Differences between conditions were evaluated using a one-way ANOVA and were significant at a 5% confidence level (Figure S9). In the first flood phase of the paddy soil, both Fh and 5% FBC6 significantly decreased pore water As concentrations compared to the control, and 5% FBC6 led to As concentrations that were significantly lower than the Fh-amended system (Fig. 5D). However, in the second flood phase, only 5% FBC6 and Fh led to significantly lower As concentrations than the control (Figure S9). These results demonstrate that both 5% FBC6 and Fh amendment are effective at immobilizing As under anaerobic soil conditions and that 5% FBC6 exhibited greater longevity by causing a statistically significant difference from the control at the end of the second flood phase.

In the orchard soil, 5% FBC6, 5% FBC3, and Fh amendments all led to lower dissolved As concentrations than the control in the first flood phase, with the 5% FBC6 and the Fh amendments significantly lower than 5% FBC3 (Figure S9). In the second flood phase, 5% FBC6 and Fh maintained better As removal compared to the control and 5% FBC3, but 5% FBC6 led to dissolved As concentrations that were now significantly lower than the Fh-amended system (Figure S9). The 5% FBC3 was no longer significantly different than the control, reflecting poor longevity of FBC3 following incubation under reducing conditions in the orchard soil. The 5% FBC6 had very similar performance in the first and second flood phases, decreasing dissolved As concentrations compared to the control by 54% and 56%, respectively. In contrast, the performance of Fh declined markedly between the first and second flood phases, where dissolved As concentrations were 64% lower in the first flood phase but were only 40% lower in the second flood phase. The superior performance of FBC6 after two flood phases in both soils compared to FBC3 and Fh amendments suggests that FBC6 has greater longevity as an adsorbent in flooded soil conditions. It is notable that the FBCs served as effective As adsorbents in the more complex pore water matrix of the soil incubations, including phosphate (Figure S10) which is known to compete with As for sorption onto FBC (Hu et al. 2015).

### The impact of flooded soil incubation on Fe morphology and speciation on BC surfaces

In order to understand the greater longevity of FBC6, FBC samples were retrieved at different stages of the flooded soil experiment and analyzed with SEM-EDS (Fig. 2E) and ATR-FTIR (Figure S11). SEM analysis of FBC6 showed that BC pores remained filled with Fe after the second flood phase, suggesting that Fe was stable through two flood phases and was not significantly depleted by reductive dissolution (Fig. 2E). FTIR analysis showed that Gt-associated peaks (891, 792, 693, 455, 388, and 259 $cm^{-1}$) were shifted to higher wavenumbers ($\Delta = +4$ to 13 $cm^{-1}$) that may indicate larger particles with a higher crystalline order after aging in redox-dynamic soil (Sklute et al. 2018, Udvardi et al. 2017). This is consistent with Thompson et al. (2006), who found multiple redox cycles in a soil transformed short-range-ordered nano-goethite to micro-crystalline goethite. In FBC6, Fh-associated peaks at 1338, 682, 427, and 263 $cm^{-1}$ were suppressed, likely due to transformation to a more stable Fe oxyhydroxide such as goethite and/or reductive dissolution of ferrihydrite phase during anaerobic periods (Aeppli et al. 2019, Erbs et al. 2010, Huang et al. 2015). In addition, the SEM images of aged FBC3 and FBC6 (Fig. 2E, F) also explain differences in longevity between these FBCs. The Fe morphology and surface distribution in FBC6 were similar before and after incubation in soil, with Fe that was well distributed in the pore structure of FBC6 before and after the flooding event (Fig. 2A, E).

## Conclusion

This study addressed a gap in the existing literature on Fe-modified biochars by systematically evaluating how variables including impregnation media pH, media Fe concentrations, and pyrolysis sequence impact FBC physiochemical properties and adsorbent performance for As(V), As(III), and Cd. FBC6 had the best performance on arsenic adsorption, with $Q_{max}$ for As(V) and As(III) at 4830 and 11,166 μg $g^{-1}$. FBC3 prepared under alkaline condition had the highest Cd adsorption capacity, with a $Q_{max}$ for Cd(II) at 3053 μg $g^{-1}$. Amorphous Fe content was the most important factor controlling the As adsorption capacity, and acidic impregnation conditions in conjunction with ultrasonic treatment led to the highest amorphous Fe loading. The morphology and surface distribution of the loaded Fe also proved to be an important determinant of As(III) and As(V) adsorption capacity, as well as the longevity of adsorbent performance. The uniform distribution and uptake of Fe into the BC pore structure led to better As(III) adsorption capacity and greater longevity, while discrete Fe aggregates on the BC surface led to better As(V) adsorption and poor longevity.

The longevity and regeneration of Fe-modified biochars were evaluated. FBC6 was effective at decreasing dissolved As concentrations in pore water over two multi-week flooded periods, decreasing pore water As by 54% and 56%, respectively, compared with the control groups in orchard soil. While the effectiveness of ferrihydrite decreased from 64 to 40% in the second flooded phase, FBC 3 showed no significant differences with control groups in the orchard soil

in the second flooded phase, indicating poor longevity and regeneration. The superior performance of FBC6 compared to FBC3 for immobilization of As in the soil microcosm studies was consistent with adsorption isotherm experiments showing that FBC3 had a higher capacity for both As(V) and As(III), and its significantly greater capacity for As(III) could be an asset in reducing soils where As(III) will be an important species. We suggest that the better longevity of FBC6 compared to FBC3 and Fh may be related to the distinct morphology of FBC6 and the uptake of Fe into the pore structure, which SEM analysis revealed to be stable after two flood periods. There was also FTIR evidence of a chemical C-O-Fe binding mechanism in FBC6, potentially giving the Fe(III) more stability in reducing conditions compared to Fe (oxy)hydroxide precipitates on the BC surface. In contrast, Fe in FBC3 was primarily in the form of crystalline goethite precipitated on the BC surface, as supported by SEM imaging showing large surficial aggregates (Fig. 2B, F). Our systematic analysis of Fe impregnation methods showed that the combination of acidic impregnation pH and sonication significantly improved the adsorption capacity for As(V) and As(III), while maintaining an intermediate capacity for Cd. These impregnation conditions also produced an FBC that was stable under consecutive flooded, anaerobic periods, indicating the potential for long-term effectiveness of FBCs in flooded rice paddy soils.

**Supplementary Information** The online version contains supplementary material available at https://doi.org/10.1007/s11356-024-33359-x.

**Acknowledgements** The authors thank J. Rohila and A. McClung for providing the rice paddy soil from Stuttgart, Arkansas, and M. McBride for assisting with collection of the orchard soil in Ithaca, NY, USA.

**Author contribution** Yi Sang: conceptualization, investigation, methodology, formal analysis, visualization, and writing—original draft preparation; Behrooz Azimzadeh: formal analysis, visualization, investigation, and writing—original draft preparation; Jessica Olsen: investigation; Jessica Rappaport: investigation; Scott C. Maguffin: investigation; Carmen Enid Martinez: conceptualization and formal analysis; Matthew C. Reid: conceptualization, formal analysis, resources, supervision, project administration, and writing—review and editing.

**Funding** This research was supported by the Cornell Center for Materials (CCMR) Research-Jump Start Program, in cooperation with B9 Plastics. This work made use of the Cornell Center for Materials Research Shared Facilities which are supported through the NSF MRSEC program (DMR-1719875) and was partially supported through the CCMR Research Experience for Undergraduates program (DMR-1757420 and DMR-1719875).

## Declarations

**Ethical approval** Not applicable.

**Consent to participate** Not applicable.

**Consent to publish** Not applicable.

**Competing interests** The authors declare no competing interests.

## References

Abdelrhman F, Gao J, Ali U, Wan N, Hu H (2022) Assessment of goethite-combined/modified biochar for cadmium and arsenic remediation in alkaline paddy soil. Environ Sci Pollut Res Int 29:40745–40754

Aeppli M, Vranic S, Kaegi R, Kretzschmar R, Brown AR, Voegelin A, Hofstetter TB, Sander M (2019) Decreases in iron oxide reducibility during microbial reductive dissolution and transformation of ferrihydrite. Environ Sci Technol 53:8736–8746

Alchouron J, Navarathna C, Chludil HD, Dewage NB, Perez F, Hassan EB, Pittman CU, Vega AS, Mlsna TE (2020) Assessing South American Guadua chacoensis bamboo biochar and Fe3O4 nanoparticle dispersed analogues for aqueous arsenic(V) remediation. Sci Total Environ 706:135943

Antelo J, Avena M, Fiol S, López R, Arce F (2005) Effects of pH and ionic strength on the adsorption of phosphate and arsenate at the goethite–water interface. J Colloid Interface Sci 285:476–486

Baig SA, Zhu J, Muhammad N, Sheng T, Xu X (2014) Effect of synthesis methods on magnetic Kans grass biochar for enhanced As(III, V) adsorption from aqueous solutions. Biomass Bioenergy 71:299–310

Baltpurvins KA, Burns RC, Lawrance GA, Stuart AD (1996) Effect of pH and anion type on the aging of freshly precipitated iron (III) hydroxide sludges. Environ Sci Technol 30:939–944

Bazilevskaya E, Archibald DD, Martínez CE (2018) Mineral colloids mediate organic carbon accumulation in a temperate forest Spodosol: depth-wise changes in pore water chemistry. Biogeochemistry 141:75–94

Bhattacharyya A, Schmidt MP, Stavitski E, Azimzadeh B, Martínez CE (2019) Ligands representing important functional groups of natural organic matter facilitate Fe redox transformations and resulting binding environments. Geochim. Cosmochim Acta 251:157–175

Blanch AJ, Quinton JS, Lenehan CE, Pring A (2008) The crystal chemistry of Al-bearing goethites: an infrared spectroscopic study. Mineral Mag 72:1043–1056

Braghiroli FL, Calugaru IL, Gonzalez-Merchan C, Neculita CM, Bouafif H, Koubaa A (2020) Efficiency of eight modified materials for As(V) removal from synthetic and real mine effluents. Miner Eng 151:106310

Calderón FJ, McCarty GW, Reeves JB (2006) Pyrolisis-MS and FT-IR analysis of fresh and decomposed dairy manure. J Anal Appl Pyrolysis 76:14–23

Calugaru IL, Neculita CM, Genty T, Zagury GJ (2019) Removal efficiency of As(V) and Sb(III) in contaminated neutral drainage by Fe-loaded biochar. Environ Sci Pollut Res Int 26:9322–9332

Cantrell KB, Hunt PG, Uchimiya M, Novak JM, Ro KS (2012) Impact of pyrolysis temperature and manure source on physicochemical characteristics of biochar. Bioresour Technol 107:419–428

Carrott P, Carrott MR, Guerrero C, Delgado L (2008) Reactivity and porosity development during pyrolysis and physical activation in CO2 or steam of kraft and hydrolytic lignins. J Anal Appl Pyrolysis 82:264–271

Cha JS, Park SH, Jung S-C, Ryu C, Jeon J-K, Shin M-C, Park Y-K (2016) Production and utilization of biochar: a review. J Ind Eng Chem 40:1–15

Chen M, Tao X, Wang D, Xu Z, Xu X, Hu X, Xu N, Cao X (2019a) Facilitated transport of cadmium by biochar-Fe3O4 nanocomposites in water-saturated natural soils. Sci Total Environ 684:265–275

Chen QY, DesMarais T, Costa M (2019b) Metals and mechanisms of carcinogenesis. Annu Rev Pharmacol Toxicol 59:537–554
Cline JD (1969) Spectrophotometric determination of hydrogen sulfide in natural waters Limnol. Oceangr. 14:454–458
Cornell RM, Schwertmann U (2003) The iron oxides: structure, properties, reactions, occurrences, and uses. John Wiley & Sons, New York
Dixit S, Hering JG (2003) Comparison of arsenic(V) and arsenic(III) sorption onto iron oxide minerals: implications for arsenic mobility. Environ Sci Technol 37:4182–4189
El-Naggar A, Lee SS, Rinklebe J, Farooq M, Song H, Sarmah AK, Zimmerman AR, Ahmad M, Shaheen SM, Ok YS (2019) Biochar application to low fertility soils: a review of current status, and future prospects. Geoderma 337:536–554
Erbs JJ, Berquó TS, Reinsch BC, Lowry GV, Banerjee SK, Penn RL (2010) Reductive dissolution of arsenic-bearing ferrihydrite. Geochim Cosmochim Acta 74:3382–3395
Fan J, Xu X, Ni Q, Lin Q, Fang J, Chen Q, Shen X, Lou L (2018) Enhanced As (V) removal from aqueous solution by biochar prepared from iron-impregnated corn straw. J Chem 2018:1–8
Fulda B, Voegelin A, Kretzschmar R (2013) Redox-controlled changes in cadmium solubility and solid-phase speciation in a paddy soil as affected by reducible sulfate and copper. Environ Sci Technol 47:12775–12783
Furcas FE, Lothenbach B, Isgor OB, Mundra S, Zhang Z, Angst UM (2022) Solubility and speciation of iron in cementitious systems. Cement Concrete Res 151:106620
Giménez J, Martínez M, de Pablo J, Rovira M, Duro L (2007) Arsenic sorption onto natural hematite, magnetite, and goethite. J Hazard Mater 141:575–580
Gong H, Zhao L, Rui X, Hu J, Zhu N (2022) A review of pristine and modified biochar immobilizing typical heavy metals in soil: applications and challenges. J Hazard Mater 432:128668
Guo J, Yan C, Luo Z, Fang H, Hu S, Cao Y (2019) Synthesis of a novel ternary HA/Fe-Mn oxides-loaded biochar composite and its application in cadmium(II) and arsenic(V) adsorption. J Environ Sci (China) 85:168–176
Hartley W, Edwards R, Lepp NW (2004) Arsenic and heavy metal mobility in iron oxide-amended contaminated soils as evaluated by short- and long-term leaching tests. Environ Pollut 131:495–504
He R, Peng Z, Lyu H, Huang H, Nan Q, Tang J (2018) Synthesis and characterization of an iron-impregnated biochar for aqueous arsenic removal. Sci Total Environ 612:1177–1186
Heiri O, Lotter AF, Lemcke G (2001) Loss on ignition as a method for estimating organic and carbonate content in sediments: reproducibility and comparability of results. J Paleolimnol 25(1):101–110
Hu X, Ding Z, Zimmerman AR, Wang S, Gao B (2015) Batch and column sorption of arsenic onto iron-impregnated biochar synthesized through hydrolysis. Water Res 68:206–216
Huang F-G, Jia S-Y, Liu Y, Wu S-H, Han X (2015) Reductive dissolution of ferrihydrite with the release of As(V) in the presence of dissolved S(-II). J Hazard Mater 286:291–297
Huang Y, Gao M, Deng Y, Khan ZH, Liu X, Song Z, Qiu W (2020) Efficient oxidation and adsorption of As(III) and As(V) in water using a Fenton-like reagent, (ferrihydrite)-loaded biochar. Sci Total Environ 715:136957
Jeong HY, Klaue B, Blum JD, Hayes KF (2007) Sorption of mercuric ion by synthetic nanocrystalline mackinawite (FeS). Environ Sci Technol 41:7699–7705
Ji L, Shao Y, Xu Z, Zheng S, Zhu D (2010) Adsorption of monoaromatic compounds and pharmaceutical antibiotics on carbon nanotubes activated by KOH etching. Environ Sci Technol 44:6429–6436
Jin H, Capareda S, Chang Z, Gao J, Xu Y, Zhang J (2014) Biochar pyrolytically produced from municipal solid wastes for aqueous As(V) removal: adsorption property and its improvement with KOH activation. Bioresour Technol 169:622–629
Jolivet J-P, Chanéac C, Tronc E (2004) Iron oxide chemistry. From molecular clusters to extended solid networks. Chem Commun 481–483. https://doi.org/10.1039/B304532N
Kassaee MZ, Motamedi E, Majdi M (2011) Magnetic Fe3O4-graphene oxide/polystyrene: fabrication and characterization of a promising nanocomposite. Chem Eng J 172:540–549
Khan ZH, Gao M, Qiu W, Islam MS, Song Z (2020) Mechanisms for cadmium adsorption by magnetic biochar composites in an aqueous solution. Chemosphere 246:125701
Kim J, Song J, Lee S-M, Jung J (2019) Application of iron-modified biochar for arsenite removal and toxicity reduction. J Ind Eng Chem 80:17–22
Kubier A, Wilkin RT, Pichler T (2019) Cadmium in soils and groundwater: a review. Appl Geochem 108:1–16
Kumar A, Gurian PL, Bucciarelli-Tieger RH, Mitchell-Blackwood J (2008) Iron oxide–coated fibrous sorbents for arsenic removal. J-Am Water Works Assoc 100:151-A4
Lata S, Prabhakar R, Adak A, Samadder SR (2019) As(V) removal using biochar produced from an agricultural waste and prediction of removal efficiency using multiple regression analysis. Environ Sci Pollut Res Int 26:32175–32188
Lehmann J, Joseph S (2015) Biochar for environmental management: science, technology and implementation. Routledge
Lehmann J, Rillig MC, Thies J, Masiello CA, Hockaday WC, Crowley D (2011) Biochar effects on soil biota – a review. Soil Biol Biochem 43:1812–1836
Li B, Yang L, Wang C-Q, Zhang Q-P, Liu Q-C, Li Y-D, Xiao R (2017) Adsorption of Cd(II) from aqueous solutions by rape straw biochar derived from different modification processes. Chemosphere 175:332–340
Li H, Dong X, da Silva EB, de Oliveira LM, Chen Y, Ma LQ (2017) Mechanisms of metal sorption by biochars: biochar characteristics and modifications. Chemosphere 178:466–478
Li C, Zhou K, Qin W, Tian C, Qi M, Yan X, Han W (2019) A review on heavy metals contamination in soil: effects, sources, and remediation techniques. Soil Sediment Conta An Int J 28:380–394
Luo M, Lin H, He Y, Li B, Dong Y, Wang L (2019) Efficient simultaneous removal of cadmium and arsenic in aqueous solution by titanium-modified ultrasonic biochar. Bioresour Technol 284:333–339
Lyu H, Tang J, Cui M, Gao B, Shen B (2020) Biochar/iron (BC/Fe) composites for soil and groundwater remediation: synthesis, applications, and mechanisms. Chemosphere 246:125609
Maguffin SC, Abu-Ali L, Tappero RV, Pena J, Rohila JS, McClung AM, Reid MC (2020) Influence of manganese abundances on iron and arsenic solubility in rice paddy soils. Geochim. Cosmochim. Acta 276:50–69
Rahman HL, Erdem H, Sahin M, Erdem M (2020) Iron-incorporated activated carbon synthesis from biomass mixture for enhanced arsenic adsorption. Water Air Soil Poll 231:1–17
Rahman MA, Lamb D, Rahman MM, Bahar MM, Sanderson P (2022) Adsorption-desorption behavior of arsenate using single and binary iron-modified biochars: thermodynamics and redox transformation. ACS Omega 7:101–117
Regmi P, Garcia Moscoso JL, Kumar S, Cao X, Mao J, Schafran G (2012) Removal of copper and cadmium from aqueous solution using switchgrass biochar produced via hydrothermal carbonization process. J Environ Manage 109:61–69
Richards BK, Steenhuis TS, Peverly JH, McBride MB (1998) Metal mobility at an old, heavily loaded sludge application site. Environ Pollut 99:365–377

Sajjadi B, Chen W-Y, Adeniyi A, Mattern DL, Mobley J, Huang C-P, Fan R (2019) Variables governing the initial stages of the synergisms of ultrasonic treatment of biochar in water with dissolved CO2. Fuel 235:1131–1145

Samsuri AW, Sadegh-Zadeh F, Seh-Bardan BJ (2013) Adsorption of As(III) and As(V) by Fe coated biochars and biochars produced from empty fruit bunch and rice husk. J Environ Chem Engineering 1:981–988

Schwertmann U, Murad E (1983) Effect of pH on the formation of goethite and hematite from ferrihydrite. Clays and Clay Minerals 31:277–284

Seyfferth AL, McCurdy S, Schaefer MV, Fendorf S (2014) Arsenic concentrations in paddy soil and rice and health implications for major rice-growing regions of Cambodia. Environ Sci Technol 48:4699–4706

Singh P, Sarswat A, Pittman CU, Mlsna T, Mohan D (2020) Sustainable low-concentration arsenite [As(III)] removal in single and multicomponent systems using hybrid iron oxide–biochar nanocomposite adsorbents—a mechanistic study. ACS Omega 5:2575–2593

Sklute EC, Kashyap S, Dyar MD, Holden JF, Tague T, Wang P, Jaret SJ (2018) Spectral and morphological characteristics of synthetic nanophase iron (oxyhydr)oxides. Phys Chem Miner 45:1–26

Smith SJ, Page K, Kim H, Campbell BJ, Boerio-Goates J, Woodfield BF (2012) Novel synthesis and structural analysis of ferrihydrite. Inorgan Chem 51:6421–6424

Sparks D (2003) Environmental soil chemistry. Elsevier

Sun Y, Yu IKM, Tsang DCW, Cao X, Lin D, Wang L, Graham NJD, Alessi DS, Komárek M, Ok YS, Feng Y, Li X-D (2019) Multifunctional iron-biochar composites for the removal of potentially toxic elements, inherent cations, and hetero-chloride from hydraulic fracturing wastewater. Environ Int 124:521–532

Sun Y, Wang T, Bai L, Han C, Sun X (2022) Application of biochar-based materials for remediation of arsenic contaminated soil and water: preparation, modification, and mechanisms. J Environ Chem Eng 10:108292

Sun Y, Yu F, Han C, Houda C, Hao M, Wang Q (2022) Research progress on adsorption of arsenic from water by modified biochar and its mechanism: a review. Water (Basel) 14:1691

Tan X, Liu Y, Zeng G, Wang X, Hu X, Gu Y, Yang Z (2015) Application of biochar for the removal of pollutants from aqueous solutions. Chemosphere 125:70–85

Tan X-F, Zhu S-S, Wang R-P, Chen Y-D, Show P-L, Zhang F-F, Ho S-H (2021) Role of biochar surface characteristics in the adsorption of aromatic compounds: pore structure and functional groups. Chin Chem Lett 32:2939–2946

Thompson A, Chadwick OA, Rancourt DG, Chorover J (2006) Iron-oxide crystallinity increases during soil redox oscillations. Geochim Cosmochim Acta 70:1710–1727

Udovic M, McBride MB (2012) Influence of compost addition on lead and arsenic bioavailability in reclaimed orchard soil assessed using Porcellio scaber bioaccumulation test. J Hazard Mater 205–206:144–149

Udvardi B, Kovács IJ, Fancsik T, Kónya P, Bátori M, Stercel F, Falus G, Szalai Z (2017) Effects of particle size on the attenuated total reflection spectrum of minerals. Appl Spectrosc 71:1157–1168

Wu C, Cui M, Xue S, Li W, Huang L, Jiang X, Qian Z (2018) Remediation of arsenic-contaminated paddy soil by iron-modified biochar. Environ Sci Poll Res 25:20792–20801

Xu Y, Xie X, Feng Y, Ashraf MA, Liu Y, Su C, Qian K, Liu P (2020) As(III) and As(V) removal mechanisms by Fe-modified biochar characterized using synchrotron-based X-ray absorption spectroscopy and confocal micro-X-ray fluorescence imaging. Bioresour Technol 304:122978

Xu Z, Wan Z, Sun Y, Cao X, Hou D, Alessi DS, Ok YS, Tsang DCW (2021) Unraveling iron speciation on Fe-biochar with distinct arsenic removal mechanisms and depth distributions of As and Fe. Chem Eng J 425:131489

Xu Z, Yu Y, Xu X, Tsang DCW, Yao C, Fan J, Zhao L, Qiu H, Cao X (2022) Direct and indirect electron transfer routes of chromium(VI) reduction with different crystalline ferric oxyhydroxides in the presence of pyrogenic carbon. Environ Sci Technol 56:1724–1735

Yang X, Shaheen SM, Wang J, Hou D, Ok YS, Wang S-L, Wang H, Rinklebe J (2022) Elucidating the redox-driven dynamic interactions between arsenic and iron-impregnated biochar in a paddy soil using geochemical and spectroscopic techniques. J Hazard Mater 422:126808

Yin D, Wang X, Peng B, Tan C, Ma LQ (2017) Effect of biochar and Fe-biochar on Cd and As mobility and transfer in soil-rice system. Chemosphere 186:928–937

Yu H, Zou W, Chen J, Chen H, Yu Z, Huang J, Tang H, Wei X, Gao B (2019) Biochar amendment improves crop production in problem soils: a review. J Environ Manage 232:8–21

Zhang X, Reid MC (2022) Inhibition of methanogenesis leads to accumulation of methylated arsenic species and enhances arsenic volatilization from rice paddy soil. Sci Total Environ 818:151696

Zhang Y, Fan J, Fu M, Ok YS, Hou Y, Cai C (2019) Adsorption antagonism and synergy of arsenate (V) and cadmium (II) onto Fe-modified rice straw biochars. Environ Geochem Health 41:1755–1766

Zhang K, Yi Y, Fang Z (2023) Remediation of cadmium or arsenic contaminated water and soil by modified biochar: a review. Chemosphere 311:136914

Zhao F-J, McGrath SP, Meharg AA (2010) Arsenic as a food chain contaminant: mechanisms of plant uptake and metabolism and mitigation strategies. Annu Rev Plant Biol 61:535–559

Zhu S, Qu T, Irshad MK, Shang J (2020) Simultaneous removal of Cd (II) and As (III) from co-contaminated aqueous solution by α-FeOOH modified biochar. Biochar 2:81–92

Zhu S, Zhao J, Zhao N, Yang X, Chen C, Shang J (2020) Goethite modified biochar as a multifunctional amendment for cationic Cd(II), anionic As(III), roxarsone, and phosphorus in soil and water. J Clean Prod 247:119579

Zoroufchi Benis K, Motalebi Damuchali A, Soltan J, McPhedran KN (2020) Treatment of aqueous arsenic - a review of biochar modification methods. Sci Total Environ 739:139750